View metadata, citation and similar papers at core.ac.uk

brought to you by CORE

provided by Apollo

UNIVERSITY OF CAMBRIDGE

A Tool for the Spectral Analysis of the Laser Doppler Anemometer Data of the Cambridge Stratified Swirl Burner

Technical Report CUED/A-TURBO/TR.135

R. Zhou*, S. Balusamy, S. Hochgreb

Cambridge Combustion Research Centre

Department of Engineering, University of Cambridge

*rz242@cam.ac.uk

Abstract

A series of flow fields generated by a turbulent methane/air stratified swirl burner are investigated using laser Doppler anemometer (LDA). The LDA provides flow field measurements with comparatively high temporal resolutions. However, processing of the power spectral energy density (PSD) and autocorrelation functions (ACF) of the flow velocity by LDA is complicated by the random, intermittent nature of the LDA signal caused by random arrival of particles at the measuring volume. A tool is developed to overcome this difficulty and the preliminary results are presented in the present report.

1. Experimental Details

The experimental details of the present report are provided in [4][7].

2 Data processing

2.1 Data pre filtering

The probability density function (PDF) of raw samples of axial velocity component u is shown in Figure 1a. Notice that there are small bumps at both ends of the PDF, which are considered to be noise. A 4σ cut off filter is used to remove the noise.

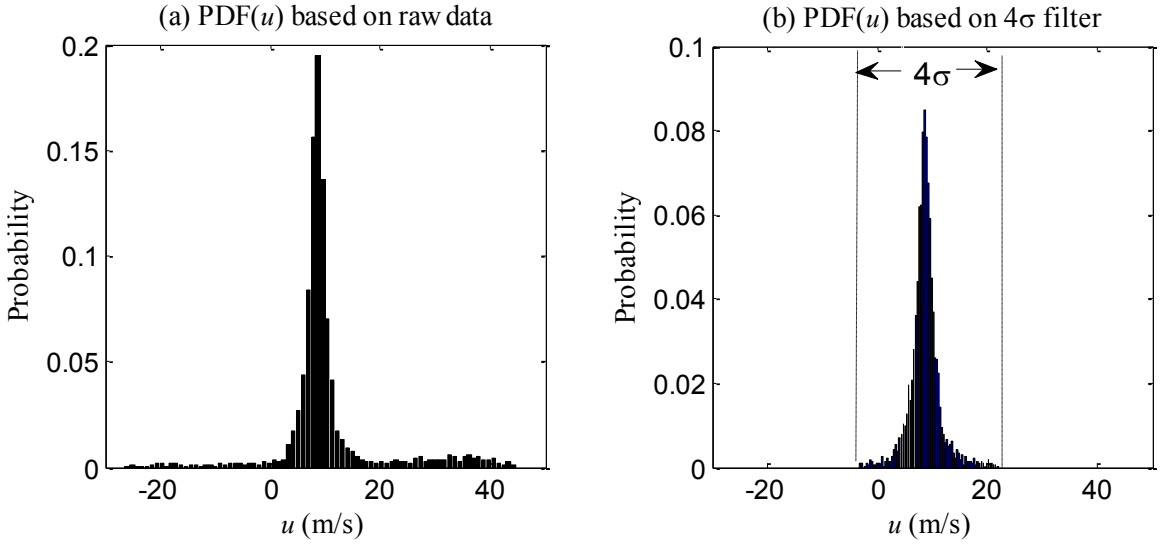

Figure 1. PDF distribution of velocity samples based on the raw data (a), and 4σ filtered data (b).

The profiles of mean axial velocities based on the raw and 4σ filtered data are shown in Figure 2. The RMS of axial velocity converges to be more symmetric by applying the 4σ filter. In

addition, the RMS peak at the location of each shear layer, i.e. r=±7, ±13 and ±18 mm, indicating that the current LDA setting can capture the general flow characteristics well. The 4σ filter is adopted as a pre processing step in the tool for calculations of the moments and power spectral density.

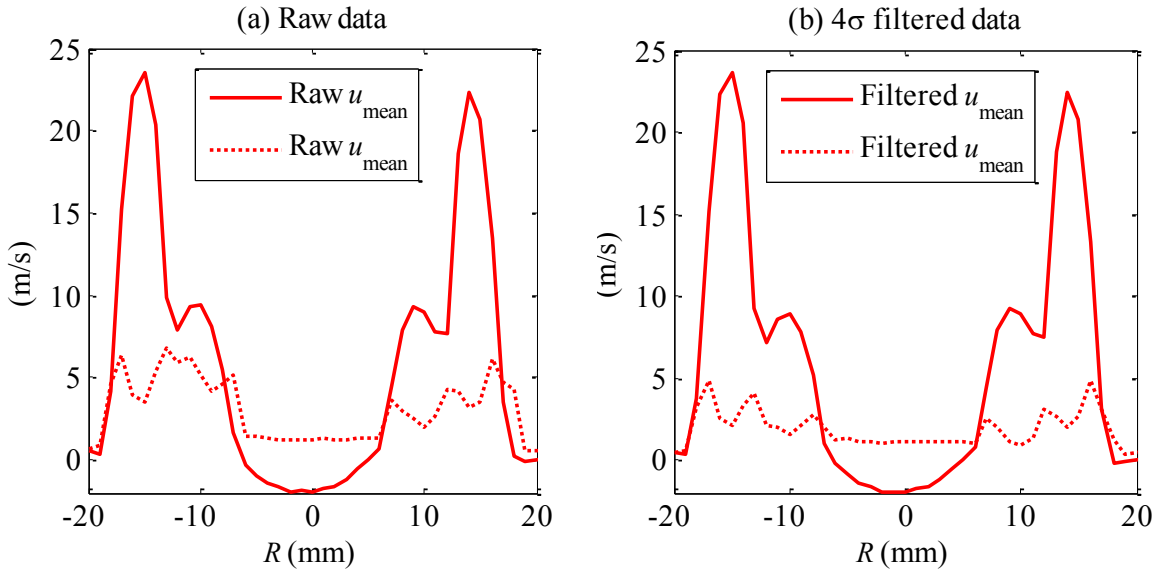

Figure 2. Filter test: profiles of mean and rms of the axial velocity based on the raw data (a), and 4σ filtered data (b).

2.2 Transit time weighting

During periods of higher velocity, a larger volume of fluid is swept through the measuring volume, and consequently a greater number of velocity samples will be recorded. As a direct result, an attempt to evaluate the statistics of the flow field using arithmetic averaging will bias the results in favor of the higher velocities.

To correct this velocity-bias, a non-uniform weighting factor η_i is introduced [2].

$$\eta_i = \frac{t_i}{\sum_{j=0}^{N-1} t_j} \tag{1}$$

-where t_i is the transit time or residence time of the i'th particle crossing the measurement volume. The transit time weighting is adopted in the tool for calculations of the moments.

2.3 Spectral analysis

The definition of the autocorrelation function is

$$R_{u\,u}(\tau) = \mathrm{E}\{u'(t_1)\cdot u'(t_2)\} \tag{2}$$

-where $\mathrm{E}\{\ldots\}$ is the notation for the expectation value (mean). The sample times t_1 and t_2 are separated by the time delay $\tau = t_2 - t_1$. Thus, the autocorrelation function (ACF) $R_{uu}(\tau)$ can be defined as:

$$R_{uu}(\tau) = \lim_{T\to\infty} \frac{1}{T} \int_0^T u'(t)u'(t+\tau)dt \tag{3}$$

-where the integration limits $0 \to T$ reflects that real measurements always take place over a finite time span.

The power density density (PSD) $S_{uu}(f)$ and the autocorrelation $R_{uu}(\tau)$ form a Fourier transform pair:

$$S_{uu}(f) = \int_{-\infty}^{\infty} R_{uu}(\tau) e^{-i2\pi f\tau} d\tau \qquad \text{(Fourier t ransform)} \tag{4}$$

$$R_{uu}(\tau) = \int_{-\infty}^{\infty} S_{uu}(f) e^{i2\pi f\tau} df \qquad \text{(Inverse Fourier tr ansform)} \tag{5}$$

The correlation theorem states that the PSD can be calculated directly from the separate Fourier transforms:

$$S_{uu}(f) = \lim_{T\to\infty} \frac{1}{T} \mathrm{E}[\mathrm{U}(-f)\mathrm{U}(f)] \tag{6}$$

-where E [...] represent the expectation value and U(*f*) represent the finite Fourier transforms of $u'(t)$:

$$\mathrm{U}(f) = \int_0^T u'(t)\, e^{-i2\pi ft}\, dt \tag{7}$$

Since $u'(t)$ is real, U(-*f*) equals $\mathrm{U}^*(f)$, with U^* representing the complex conjugate of U. The PSD can be estimated from U(*f*) directly:

$$\hat{S}_{uu}(f) = \frac{1}{T} \mathrm{U}^*(f)\, \mathrm{U}(f) \tag{8}$$

Wiener-Khinchin Theorem states that:

$$\hat{S}_{uu}(f) = \frac{1}{T} |\mathrm{U}(f)|^2 \tag{9}$$

The definitions of correlations and spectra above are based on continuous signals $u'(t)$. In contrast to the straightforward computation of power spectral density functions for continuous or equally sampled data, LDA data is randomly sampled in time and no obvious equivalent to the fast Fourier transform is available as a computational algorithm.

The present study used a sample-and-hold [1] reconstruction method to create equidistantly spaced time series, thereby allowing a FFT to be used in making PSD or ACF estimates. It can be written as

$$u(t) = u(t_i), \text{ for } t_i \le t < t_{i+1}, \text{ and } i = 1, 2, 3, \ldots, N_R \tag{10}$$

where N_R is the total number of samples in a given block of data, $u(t_i)$ and $u(t)$ are the true samples and resamples of the LDA data. The reconstruction can be performed either over the entire data set or within data blocks. The equidistant resampling with time steps of Δt_s is performed by

$$u_i = u(i\Delta t_s), \text{ for } i = 0, 1, 2, 3, \ldots, N_R \tag{11}$$

and leads to a data set of N_R samples that can be processed by a Fourier transform. The concept is well explained in Figure 3.

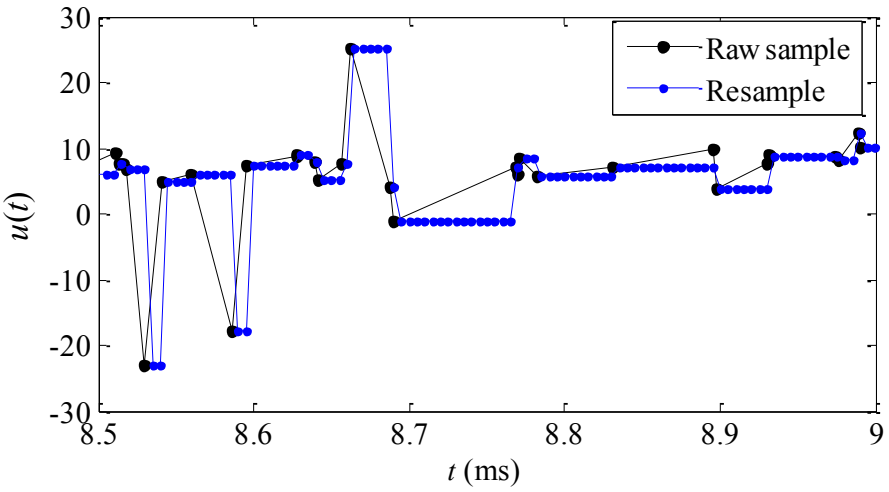

Figure 3. Random true sample and S+H Resample.

With resampled data, the integrals in equation (7) can be estimated as sums:

$$\mathrm{U}(f_k) = \Delta t_s \underbrace{\sum_{n=0}^{N_R-1} u' \exp\left(-i2\pi \frac{kn}{N_R}\right)}_{\text{FFT of } u', \text{if } N_R \text{ is a power of two}} \tag{12}$$

-where $\Delta t_s = T_b / N_R$ is the resampling interval, and each value of k represent a different frequency: $f_k=k/T_b$, k=0, 1, 2, ..., $N_R/2$. If N_R, the number of samples, is a power of two, the above expressions can be calculated using FFT-algorithms. Thus equation (9) becomes:

$$S_n = \frac{\Delta t_s}{N_R} \left| U_n' \right|^2, \text{ for } n = 0, 1, 2, ..., N_R / 2 \tag{13}$$

-where U_n' is the Fast Fourier transform (FFT) of u_i'. The integrals in Equation (5) can be estimated as sums:

$$R = \Delta f \underbrace{\sum_{n=0}^{N_R-1} S_n \exp\left(i 2\pi \frac{kn}{N_R} \right)}_{IFFT\ of\ S_n\ ,if\ N_R\ is\ a\ power\ of\ two} \tag{14}$$

-where Δf is the resampling frequency interval. If N_R, the number of samples, is a power of two, the above expressions can be calculated using Inverse FFT-algorithms. Thus equation (14) becomes:

$$R_k = \frac{1}{N_R \cdot \Delta t_s} X_k, \text{ for } n = 0, 1, 2, \ldots, N_R/2 \tag{15}$$

-where X_k is the Inverse Fast Fourier transform (IFFT) of S_n.

The S+H method [3] has been proved to serve as a first-order, low-pass filter:

$$S_n = \frac{1}{1 + w^2 / \dot{n}^2} \left[S_{true} + \underbrace{\frac{2\sigma_u^2}{\dot{n}^3 T_\lambda^2}}_{\text{step noise}} \right] \tag{16}$$

-where $w, \dot{n}, S_{true}, \sigma_u, T_\lambda$ denote the circular frequency, resample data rate, true power spectrum, root mean value of u' and Taylor's microscale for u', respectively. Equation (16) predicts that the spectral level of the step noise within the bandpass of the low filter vanishes as $\dot{n}^{-3}$, whilst above the cut off frequency $f = w/2\pi = \dot{n}/2\pi$, it vanishes as $\dot{n}^{-1}$.

In practice, the random errors can be reduced by smoothing the estimated spectrum. The smoothing can be implemented by splitting the raw data into blocks of equal duration.

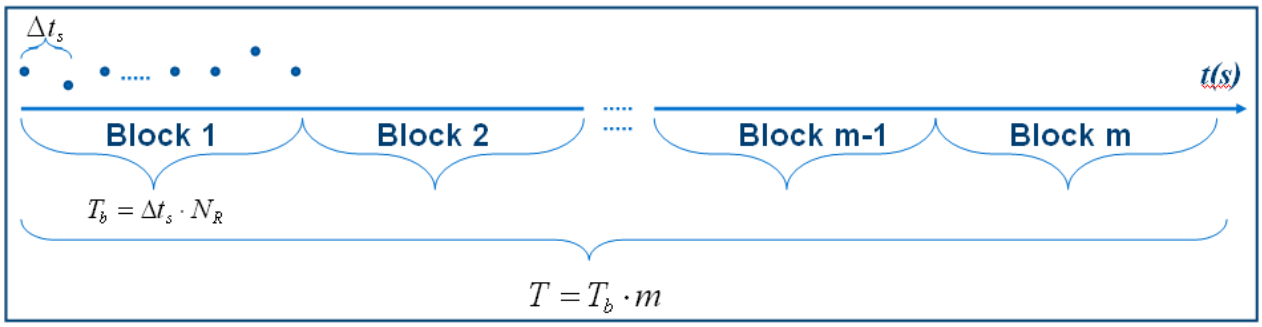

Figure 4. Block splitting and averaging technique

As illustrated in Figure 4, the entire dataset is divided into a number of blocks with equal block length. Separate PSD, S_n, and ACF, R_k, are calculated for individual block, and the final PSD and ACF are determined as the average of separate S_n and R_k:

$$S_b = \frac{1}{m}\sum_{i=1}^{m} S_n \tag{17}$$

$$R_b = \frac{1}{m}\sum_{i=1}^{m} R_k \tag{18}$$

where m is the number of blocks used in the calculation. To get as many blocks as possible within the limited duration of the experiment, short blocks are desirable. Unfortunately the frequency resolution of the calculated spectrum is inversely proportional with the duration T_b of the blocks:

$$\Delta f = \frac{1}{T_b} = \frac{1}{N_R \cdot \Delta t_s} \tag{19}$$

so the settings chosen will be a compromise between resolution and variance. The following section provides details on balancing the resolution and variance.

Integral time scales can be derived from the integration of the profiles of autocorrelation function coefficients (ACFC). The ACFC is integrated to the first zero crossing, or to the minimum of the ACFC in the absence of a zero crossing [6].

3 Processing parameters

This section discusses how the processing parameters used in the tool are optimized.

3.1 Raw PSD and Filtered PSD

This subsection presents the calculated PSD with and without Hanning filter for smoothing purpose.

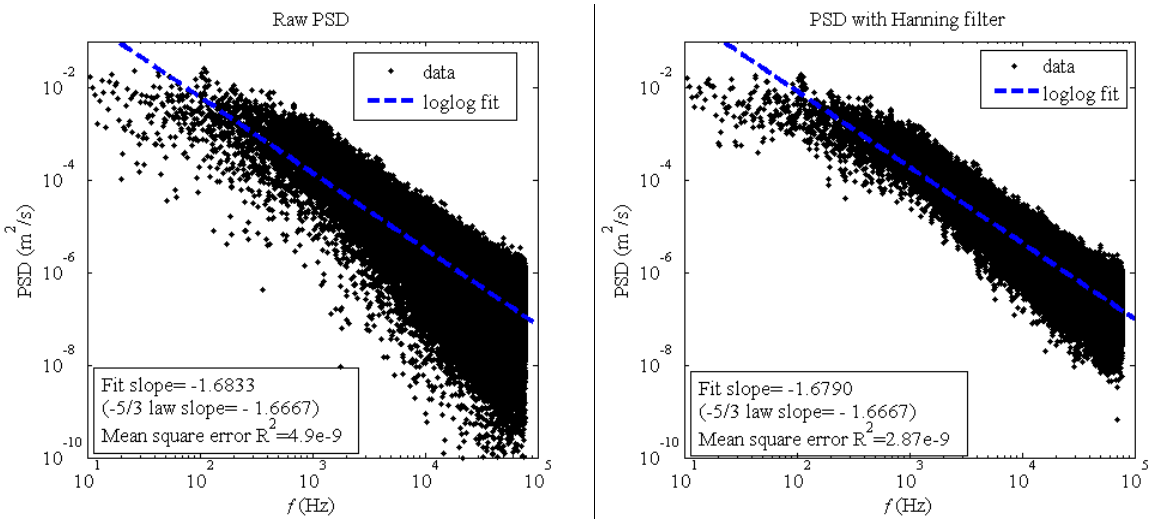

Figure 5. PSD with and without Hanning filter

The Hanning filter is used in post processing the Raw PSD and the resulted filtered PSD is presented in Figure 5. Details about Hanning filter can be found in the BSA manual [2]. Basically the effect of Hanning filter is to replace each spectrum estimate with a weighted average of the "old" estimate and its neighbors. An auto-adaptive log fit is applied to the PSD and the resulted mean square error is considered as an indicator of the variance of the estimation [5]. The results show that the variance of the spectrum estimate is significantly reduced by using the Hanning filter, without losing frequency resolutions. Thus, Hanning filter is adopted in the tool.

3.2 Resampling time interval: Δt_s

The homogeneous, but random distribution of seeding particles in the fluid results in particle arrivals following a Poisson process:

$$\mathrm{P}(k, \Delta t_s) = \frac{(\dot{n} \cdot \Delta t_s)^k}{k!} \mathrm{e}^{-\dot{n} \cdot \Delta t_s} \tag{20}$$

It represents the probability P of k particle arrivals within the period Δt_s, when the average data rate is $\dot{n}$ per second. With the resampling frequency chosen as c times the average data rate of the original samples, we get: $\Delta t_s = 1/(\mathrm{c} \cdot \dot{n}) \Leftrightarrow \dot{n} \cdot \Delta t_s = 1/\mathrm{c}$. Inserting this in Eq. (20) we can

calculate the probability of more than one particle arrival during each Δt_s:

$$\mathrm{P}(k>1) = 1 - \mathrm{P}(0) - \mathrm{P}(1) = 1 - (1+1/\mathrm{c}) \cdot \mathrm{e}^{-1/\mathrm{c}} \tag{21}$$

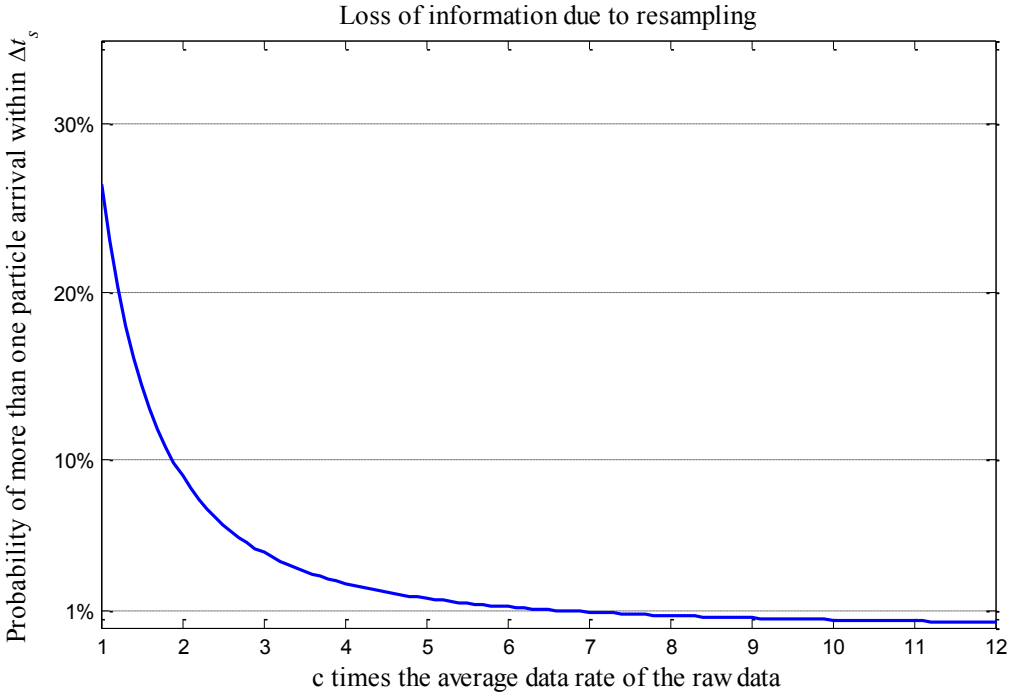

Figure 6. Probability of more than one particle arrival between two resamples as a function of the resampling rate.

Figure 6 shows the probability of having more than one particle arrival in the time between two resamples. Several particle arrivals between two resamples will cause loss of information, since only the last particle is recorded in the sample and hold method. Increasing the resampling frequency, i.e. increasing c, will reduce the width of each time-slot, and obviously reduce the risk of having more than one true sample in it. Unfortunately it also increases the probability of no particle arrival at all (as shown in Figure 3), and furthermore increase the total amount of data, requiring additional storage capacity and calculation time. Due to the random nature of particle arrivals, we can never completely avoid loss of data: even with a resampling rate of 10 times the original data rate, approximately 0.5% of the time-slots will contain two (or more) particle arrivals.

Figure 7 presents the PSD estimations based on different resampling frequencies. As the resampling frequency increases, higher frequency components could be solved with the cost of lower frequency resolution according to Eq. (19). Notice that the resampling frequency also affects the range and variance of the spectral estimation. Figure 8 shows the variance of the PSD estimation based on different resampling frequencies. Clearly the variance is reduced as the resampling frequency increases and starts to converge at c=5.

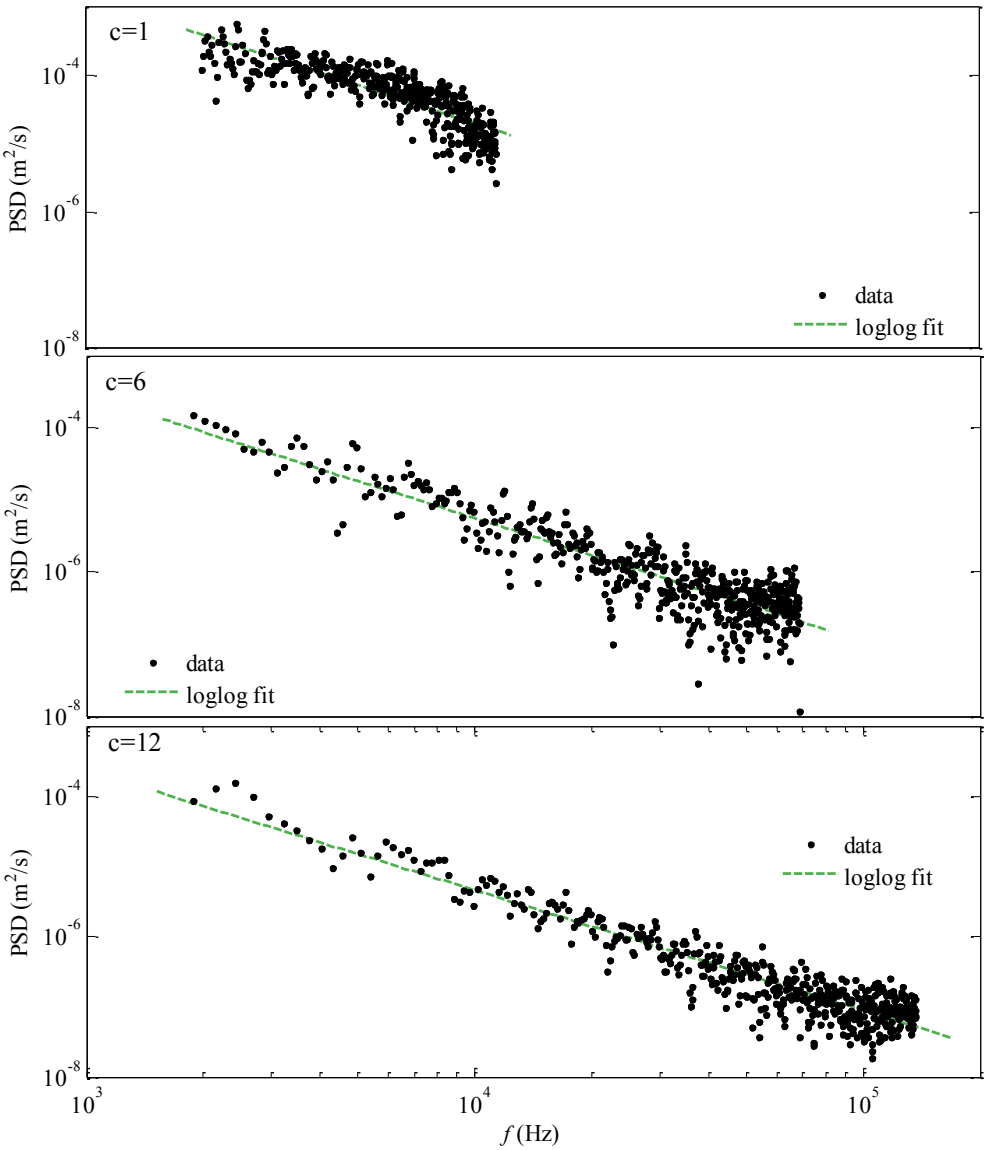

Figure 7. PSD calculations based on different resampling frequencies. The resampling frequency is increased as c increases from 1 to 12.

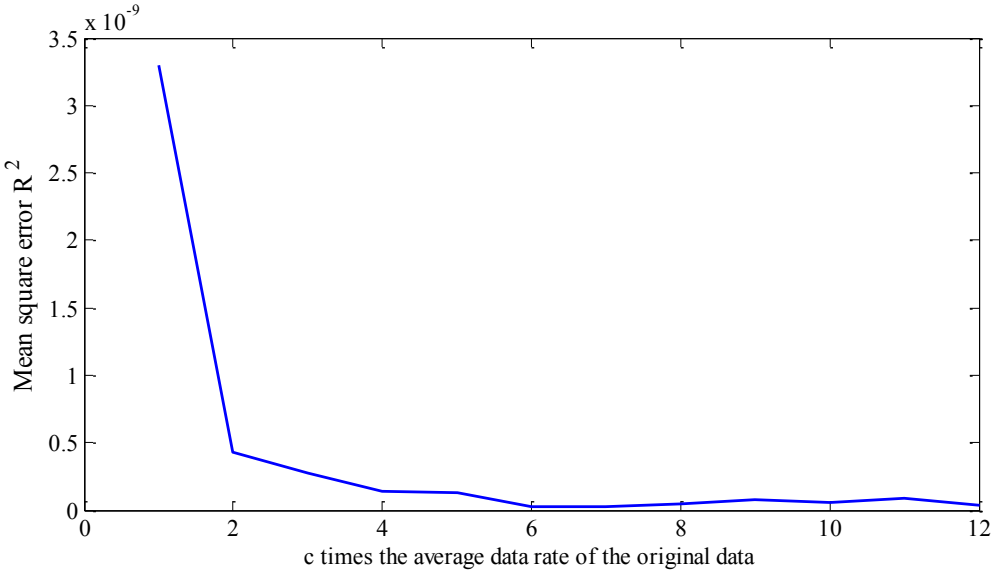

Figure 8. Variance of the estimation as a function of the resampling frequency.

The present work used a resampling rate of 7 times the original data rate, which is approximately 150 kHz (corresponding $\Delta t_s = 6.3\text{e}{-6}\,\text{s}$) at the current location *r*=8 mm, z=10 mm of *cSwB*1 case. More than 99% of the flow information could be recorded with this resampling frequency (Figure 6) and the variance is at the converged level (Figure 8).

3.3 Block length: T_b

The block length is chosen based on two factors:

1) The block length should be long enough to solve the integral time scales as well as maintaining satisfactory frequency resolutions.
2) In order to maintain a sufficient number of blocks for block averaging technique (Section 3.4), the length of each block should not be too long. This factor will be discussed together with the effect of number of blocks in Section 3.4.

3.3.1 Solving integral time scales

Only very limited information is available within each block regarding the larger time scales; in fact only a single pair (the very first and the very last sample) truly provides information regarding correlation at the desired maximum time scale. Consequently we should always select a maximum block length considerably larger than the largest time scale of real interest (i.e. integral time scale in our case): thus, the block length should be at least 10 times the integral time scale, and preferably even higher in order to obtain reliable time scale; a maximum block length of 50 times the integral time scale is not excessive.

3.3.2 Frequency resolution

The block length $T_b = N_R \cdot \Delta t_s$. With a fixed Δt_s, the effect of the block length on the frequency resolution of the spectral estimation can be investigated by varying the number of samples within the block, N_R. Figure 9 shows that the frequency resolutions of the results are enhanced by increasing N_R.

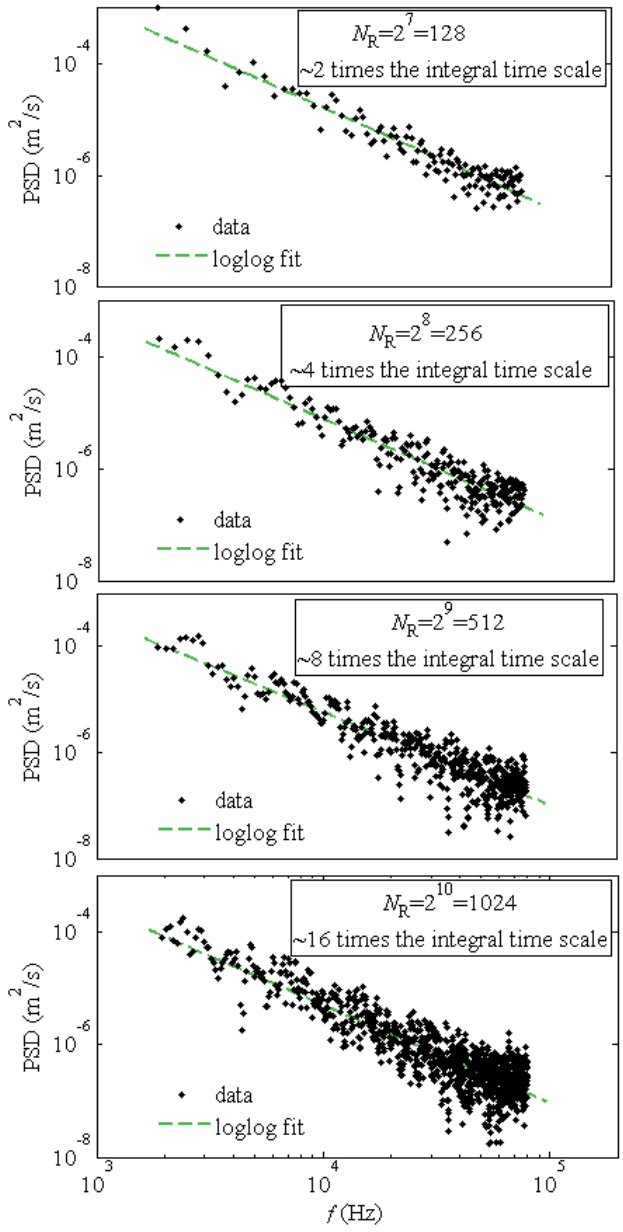

Figure 9. PSD calculations based on different N_R at a fixed Δt_s.

3.4 Number of blocks: m

The block splitting and averaging technique is used to reduce the variance of the spectrum estimate. Figure 10 presents the PSD estimations obtained by averaging different number of blocks N_B. Figure 11 shows that as the number of block increases, the variances of the PSD estimations are significantly reduced. However, increasing the block numbers also leads to shorter block length, resulting in lower frequency resolution as explained in Section 3.3.2. The present work divided the dataset into 100 blocks (corresponding $\Delta t_s = 6.3\text{e}{-6}\,\text{s}$ and N_R=1024) at the current location r=8 mm, z=10 mm of *cSwB*1 case. The PSD estimation using these parameters maintains an acceptable frequency resolution ($\Delta f / (f_{\max} - f_{\min}) < 0.001$), the capability

to solve integral time scale (Section 3.3) and a satisfactory variance level (Figure 10 and 11).

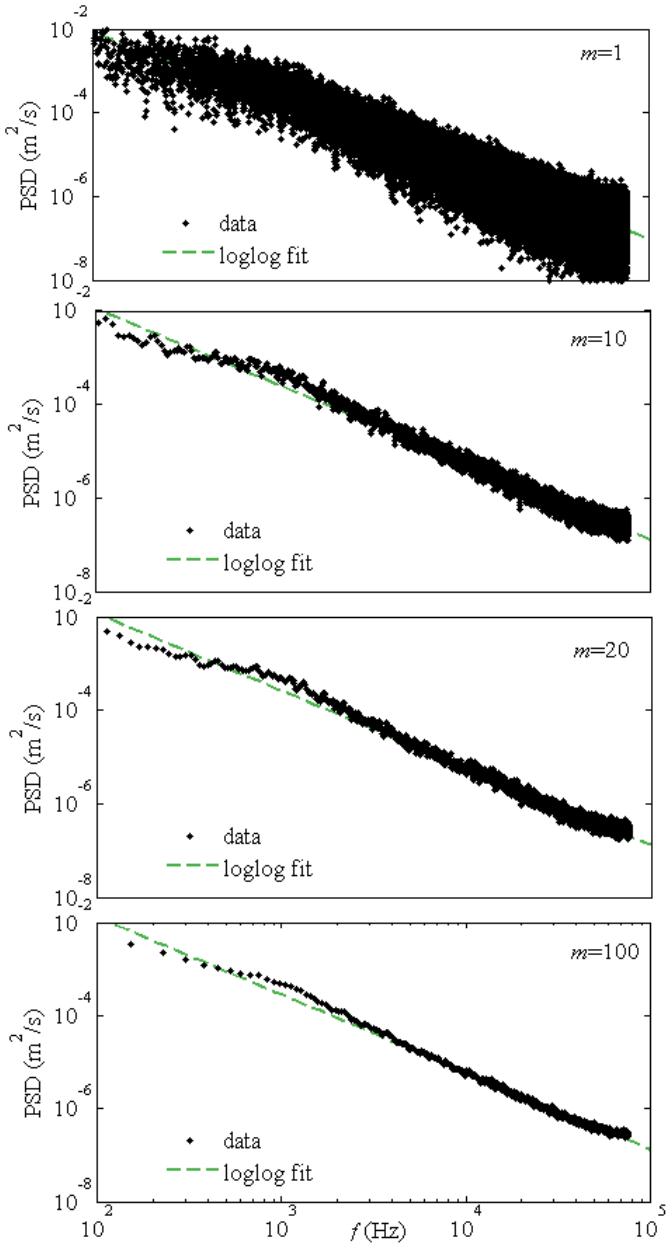

Figure 10. PSD calculations based on different number of blocks.

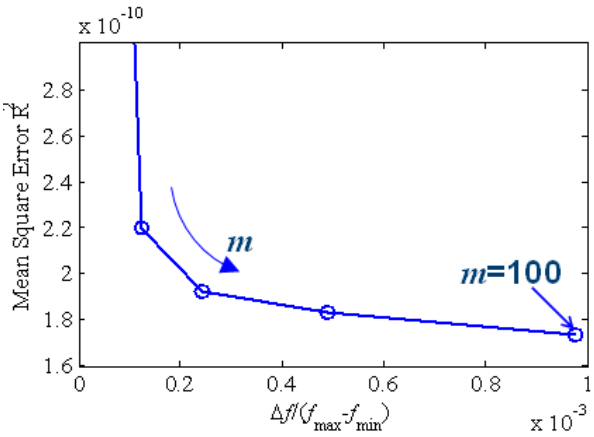

Figure 11. The mean square errors and frequency resolutions of the PSD estimations as a function of the number of blocks used to divide the dataset.

For datasets at other locations, the tool used an algorithm to make sure that the block lengths are around 15 times the integral time scales with at least 50 blocks available within the datasets.

4 Conclusions

The present work developed a robust tool to calculate the PSD from the LDA data which are irregularly spaced in time. The flow chart below shows the improvement of the results by using this tool. The ACF derived from the final PSD is smooth and good for further integration.

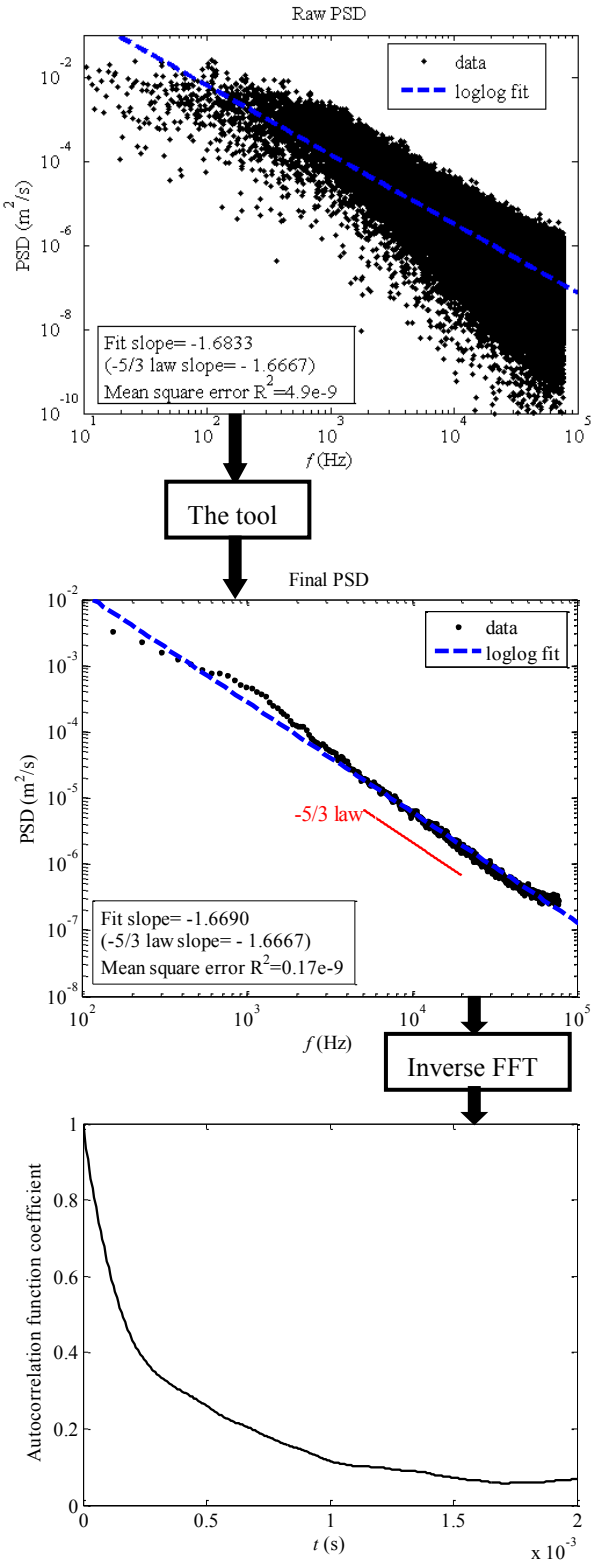

Reference:

[1] L.H. Benedict, H. Nobach, C. Tropea. *Estimation of turbulent velocity spectra from laser Doppler data*, Meas. Sci. Technol. 11, 1089–1104 (2000)

[2] Dantec Dynamics A/S. BSA Flow Software Version 4.10, 2006.

[3] R.J. Adrian, C.S. Yao. *Power spectra of fluid velocities measured by laser Doppler velocimetry*, Exp. Fluids 5, 17–28 (1987)

[4] M.S. Sweeney, S. Hochgreb, M.J. Dunn, R.S. Barlow. *The Structure of Turbulent Stratified and Premixed Methane/Air Flames II: Swirling Flows*. Combust. Flame, 2012. (Accepted)

[5] Jonathan C. Lansey. *logfit.m*, Online, URL: http://www.mathworks.com/matlabcentral/fileexchange/29545-power-law-exponential-and-logarithmic-fit, 2010.

[6] P.L. O'Neill, D. Nicolaides, D. Honnery, J. Soria. *Autocorrelation Functions and the Determination of Integral Length with Reference to Experimental and Numerical Data*. 15th Australasian Fluid Mechanics Conference, The University of Sydney, Sydney, Australia, 13-17 December 2004

[7] R. Zhou, M.S. Sweeney, S. Hochgreb. *Flow Field Results of the Cambridge Stratified Swirl Burner Using Laser Doppler Anemometer*. Technical Report CUED/A-TURBO/TR.134.
URL: http://www.dspace.cam.ac.uk/handle/1810/226463, 2012.